Research Paper

Performance of geosynthetic reinforced soil bridge abutments with modular block facing under fire scenarios

A. Yarivand [a,*], C. Behnia [a], S. Bakhtiyari [b], A. Ghalandarzadeh [a]

[a] Faculty of Civil Engineering, University of Tehran, 4563-11155 Tehran, Iran
[b] Road, Housing & Urban Development Research Center, 1696 – 13145 Tehran, Iran

ABSTRACT

This paper investigates the effect of fire on the performance of geosynthetic reinforced soil bridge abutments using experimental tests and finite element analyses. Experimental programs were comprised of a series of tensile strength tests at elevated temperatures and fire resistance tests, which were performed on a physical model. Findings revealed the adverse effect of fire on geosynthetic reinforced soil bridge abutments when fire duration exceeded 60 min. Results show that the depth within the backfill affected by the fire is approximately 50 cm.

© 2016 Elsevier Ltd. All rights reserved.

1. Introduction

In recent years, the use of the geosynthetic reinforced soil (GRS) technology for bridge abutments has been recommended because it has advantages over conventional methods. The GRS bridge abutment system includes a segmental geosynthetic reinforced soil wall with a bridge seat (sill) placed on the top of it. The stability of these structures depends on the mechanical properties of the reinforcing elements as well as their interactions with the soil. Fig. 1 shows a typical GRS bridge abutment system with modular concrete block facing.

Geosynthetic reinforcements such as geotextiles and geogrids are made from synthetic polymers and mechanical properties of the polymers change with increased temperatures. Nonlinear increases in creep, a significant reduction in tensile strength, increased failure strain, increased degradation, a reduction in the modulus of elasticity, and a reduction in surface hardness are some of the consequences of increased temperatures on the properties of these types of material [1–8]. Few attempts have been made to study the effect of temperature distribution on reinforced soil structures (due to ambient temperature variations). Segrestin and

Jailloux [9] investigated the effect of temperature variation on the geosynthetic aging and discovered that in a reinforced soil structure, the temperature within the backfill varies to a depth of 10 m. A seven-year observation of a reinforced earth structure on the M25 motorway at Waltham Cross, UK, carried out by Murray and Farrar [10]. Their observation showed that 0.3 m behind the facing, soil temperature was relatively close to ambient temperature and after a distance of almost 4 m from the nearest external boundary, the soil temperature was constant. Kasozi et al. [8] studied numerically the temperature distribution in a mechanically stabilized earth wall structure in Las Vegas, NV using field data from the Tanque-Verde MSE wall in Tucson, AZ. Based on their study, the overall average temperature within the backfill was much higher than the highlighted test in ASTM D6637 [11]. They recommended that a reduction in reinforcement strength from rising temperatures should be considered when designing reinforced soil structures. Apart from ambient temperature, one of the factors that may cause temperature to rise in reinforced soil structures is fire. Studies on the behavior of geotechnical structures when subjected to fire are not very common, possibly because the thermal conductivity of soil is low and the likelihood of mechanical properties changes of soil due to fire is low. In the case of GRS, owing to the nature of geosynthetics (as mentioned earlier), more investigation on the effect of fire on GRS performance was required. As reported in NCHRP Project 12-85 [12] (Highway Bridge Fire Hazard Assessment), structures beneath bridges that are close to the
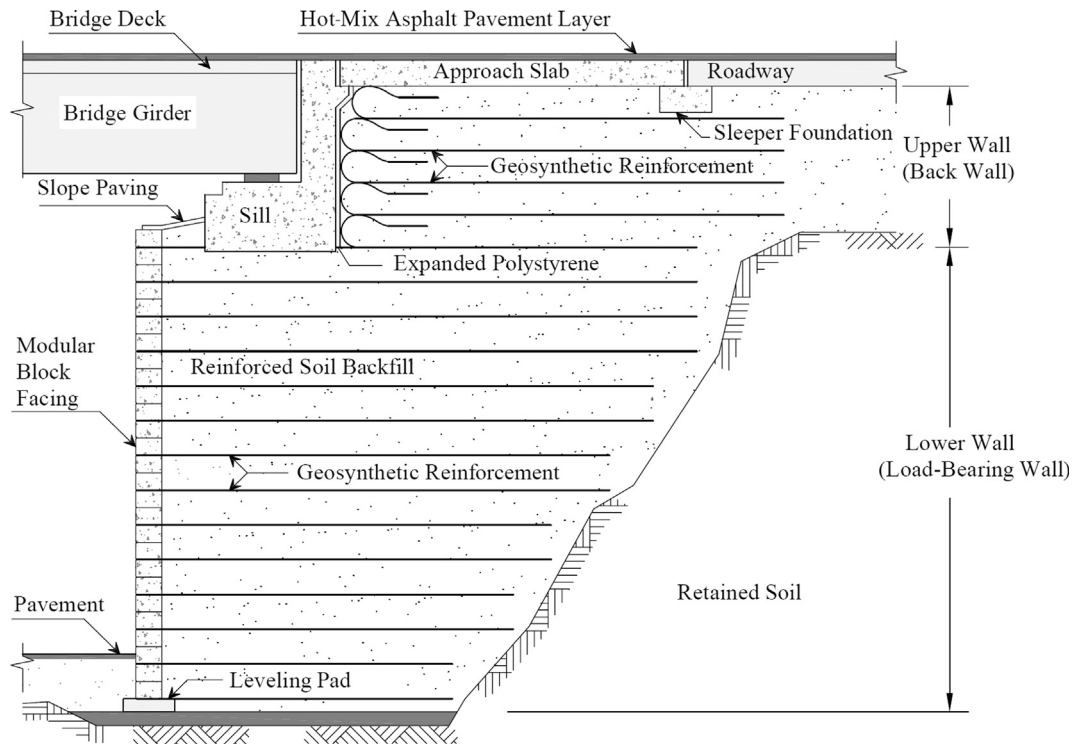
Fig. 1. Typical GRS bridge abutment system with modular concrete block facing.

roadway, like piers and abutments, were involved in many crash events that occurred underneath the bridge. Based on statistical data, half of fire events related to bridges occurred under the bridges. According to this report, two complete bridge-collapses in the United States (the MacArthur Maze freeway interchange in Oakland and the Nine Mile Road Bridge in Detroit) were caused by fuel tanker accidents (which results in huge fire). Such accidents are inevitable, making the study of GRS bridge abutments behavior when subjected to fire of importance.

Austin [13] carried out one of the few studies to investigate the effects of fire exposure on geosynthetic reinforced soil structures. In his research, two different wall configurations were tested in front of a gas furnace. The blocks used in his study were (a) a standard block and (b) a standard block with a 35 mm cavity and half brick masonry facing. As reported in his study, the fire used was in accordance with BS 476 Part 20 (British Standards Institution, 1987a). Fire testing time was 30 min. At the end of the test, when the maximum temperature of the furnace was 871 °C, the recorded temperature in the cavity (at the connector locations) was 66 °C and the temperature recorded behind the brick faced half of the test panel was 17 °C. Ambient temperature was 14 °C. Austin concluded that exposure to short-period fires does not have a significant effect on GRS structures with segmental blocks.

In recent years, GRS bridge abutment construction in Iran has gained considerable attention. Owing to a high number of road accidents, which can lead to fire near structures under bridges, the Road, Housing and Urban Development Research Center of Iran (BHRC) investigated the performance of GRS bridge abutments under possible fire scenarios. This study is part of a more comprehensive study supported by Tehran University and BHRC to evaluate the performance of GRS bridge abutments under fire conditions.

The results presented in this paper are derived from laboratory tests and numerical models. Laboratory tests included a series of tensile tests under elevated temperatures up to 140 °C for two types of geogrids as well as four fire resistance tests on a physical

model of reinforced soil structure with the modular block facing exposed to a hydrocarbon fire curve with a maximum temperature of 1100 °C. For numerical modeling, a parametric study was performed using finite elements method. Numerous researchers have identified the advantages of finite elements method (FEM) for modeling and predicting the behavior of GRS bridge abutments [14–19]. The finite element model was calibrated using measured temperature data from fire resistance tests. This calibrated model was used to predict the behavior of a 4.8 m high GRS bridge abutment under various sill pressures and different fire durations. The results of this study improve our understanding of the performance of these structures under fire loading conditions.

2. Experimental program

2.1. Materials

The sand used in physical models was a siliceous, medium to coarse, clean washed sand. The coefficient of curvature (Cc) and coefficient of uniformity (Cu) were 1.42 and 7.89, respectively. Sand grains were formed from rounded and sub-rounded particles. Using the standard index density test recommended by ASTM D4254 [20] and ASTM D4253 [21], the minimum and maximum dry unit weights of the sand were found to be 16.43 and 18.78 kN/m³, respectively. Results of direct shear tests suggest that the internal friction angle of the sand was 34°. Direct shear tests were conducted in accordance with ASTM D3080 [22]. Two types of geogrid were used, a PVC coated polyester (PET) geogrid and a uniaxial high-density polyethylene (HDPE) geogrid with ultimate tensile strengths of 40 kN/m and 45 KN/m, respectively. The physical and mechanical properties of the geogrids are presented in Table 1. Solid cast concrete blocks with dimensions of 150 mm × 150 mm × 150 mm was used as the facing element in the physical model. The 28-day compressive strength of normal concrete was almost equal to 28 MPa (according to FHWA design

Table 1
Physical and mechanical properties of geogrids.

Characteristic	Base material	
	Polyester	High-density polyethylene
Geogrid name	PET	HDPE
Aperture size (MD[a]/TD[b]) (mm)	35/25	220/16
Thickness (mm)	0.8	1.12
Mass per unit area (g/m^2)	380	300
Peak tensile strength (MD[a]/TD[b]) (KN/m)	40/20	45/-
Yield point elongation (MD[a]) (%)	11	13

[a] MD = machine direction (longitudinal to roll)
[b] TD = transverse direction (across roll width)

approach [23]). Aggregates used to make the concrete were siliceous and the dry concrete density was 23.5 kN/m^3.

2.2. Test methods

2.2.1. Elevated temperature tensile testing

A series of tensile tests at elevated temperatures were performed on PET and HDPE geogrids. The tests were conducted in accordance with ASTM D6637 test guidelines [11]. A universal testing machine (UTM) was developed at the Iran Polymer and Petrochemical Institute (IPPI) as shown in Fig. 2. The developed UTM includes a chamber, electric heating elements, an electric blower, and a temperature control system. The heating rate was 2 °C/min. Tests were conducted at standard temperature 20 °C and at higher temperatures up to 140 °C. The tests were performed at a constant strain rate of 10% per minute for one strip of the geogrids.

2.2.2. Fire resistance tests

A series of fire tests were carried out at the Fire laboratory of BHRC. Fire resistance tests are commonly used to evaluate the behavior of structural elements when exposed to a standard fire. In this study, these tests were performed to determine temperature distribution in a GRS backfill and to define the thermal characteristics of the facing and backfill. Results of these test are used (as discussed later) in FE analysis. The tests were carried out using a gas furnace used to simulate a hydrocarbon fire curve (in accordance with Eurocode 1 standard [24]) with a maximum

temperature of 1100 °C. The constructed models were 825 mm high, 825 mm wide, and 700 mm long and were comprised of a concrete block wall (facing), sandy backfill and three layers of geogrid. The configurations were constructed in a box built of steel frames. In order to reach 70 percent relative density, using a trial-and-error method, the sand was constructed in the test box in a number of layers (each layer was approximately 5 cm). The layers were compacted with the aid of a 4.5 kg hammer. The geogrids were placed in the soil with a vertical spacing of 300 mm. A horizontal joint (1–2 mm) appeared between the blocks due to geogrid installation. The model setup is shown in Fig. 3.

As shown in Fig. 3b, 16 thermocouples (type k) in 2 series, top and bottom, were placed in the soil body to record the temperatures at different distances (bottom row: 0, 5, 10, 15, 25, 35 cm, top row: 2, 4, 6, 8, 10, 12, 14, 16, 18 cm). The heating phase duration for the fire was 120 min. Maximum test time was 360 min.

2.3. Tensile and fire tests results

2.3.1. Tensile tests

The typical tensile load versus strain curves at elevated temperatures for the PET geogrid and HDPE geogrid are shown in Fig. 4. Each curve was selected from among five tests at any temperature (i.e. the middle curve was selected).

As shown in Fig. 4, ultimate tensile strength decreased as the test temperature increased. For the PET geogrid, the reduction rate for ultimate tensile strength was −0.28%/°C when the temperature increased from 20 °C to 80 °C. This result was in agreement with the results of Hsieh and Tseng [5] and Kongkitkul et al. [7] with values of −0.33%/°C and −0.225%/°C, respectively. Above 80 °C, this value was −0.46%/°C. The elongation at break for the PET geogrid varied from 10% to 12% and showed no particular trend. For the HDPE geogrid, the reduction rate of the ultimate tensile strength was −0.79%/°C when the temperature increased from 20 °C to 60 °C. This result was smaller than the results presented by Kongkitkul et al. [7] and Kasozi et al. [8] with values of −1.33%/°C. Above 60 °C, the reduction rate of the ultimate tensile strength increased to −1.06%/°C. For temperatures up to 60 °C, the elongation at break for HDPE geogrid was 0.93%/°C. From 60 °C to 80 °C, this value was 7.59%/°C. Above 80 °C, results were extremely high (the device was turned off at 100% strain).
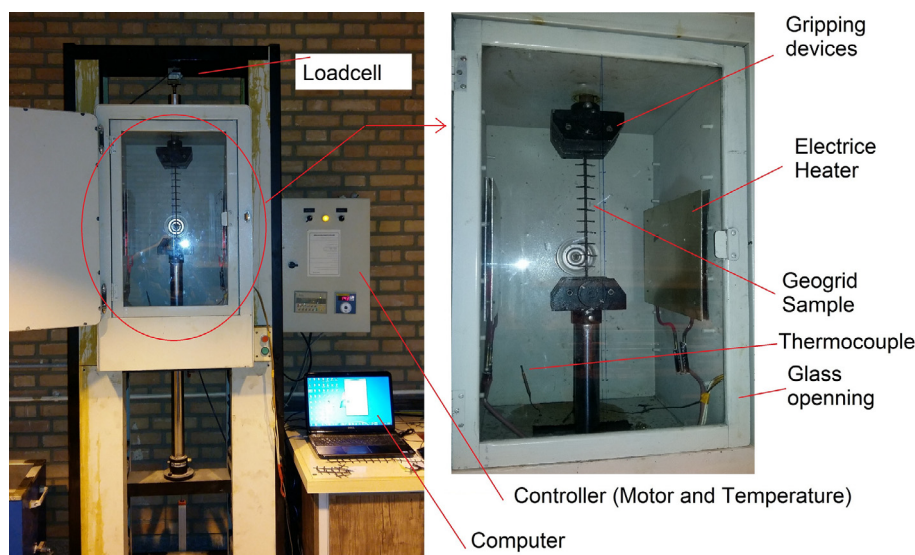

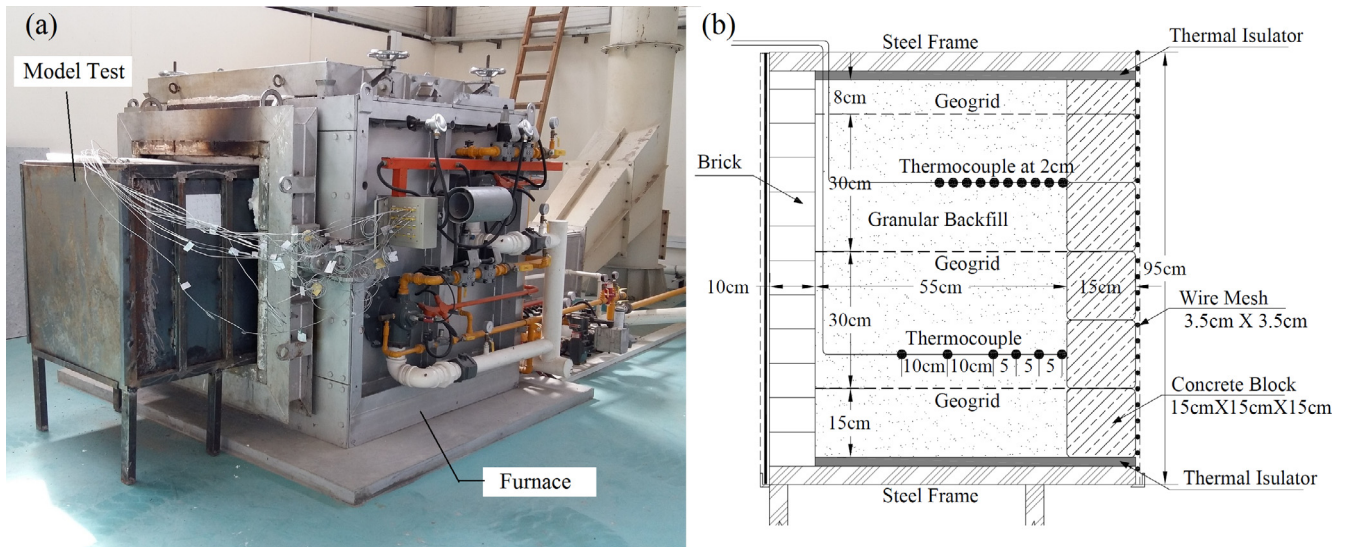**Fig. 2.** Details of tensile strength testing apparatus used in this study.

Fig. 3. (a) Setup in front of the furnace, (b) Details details of the model used in fire tests.
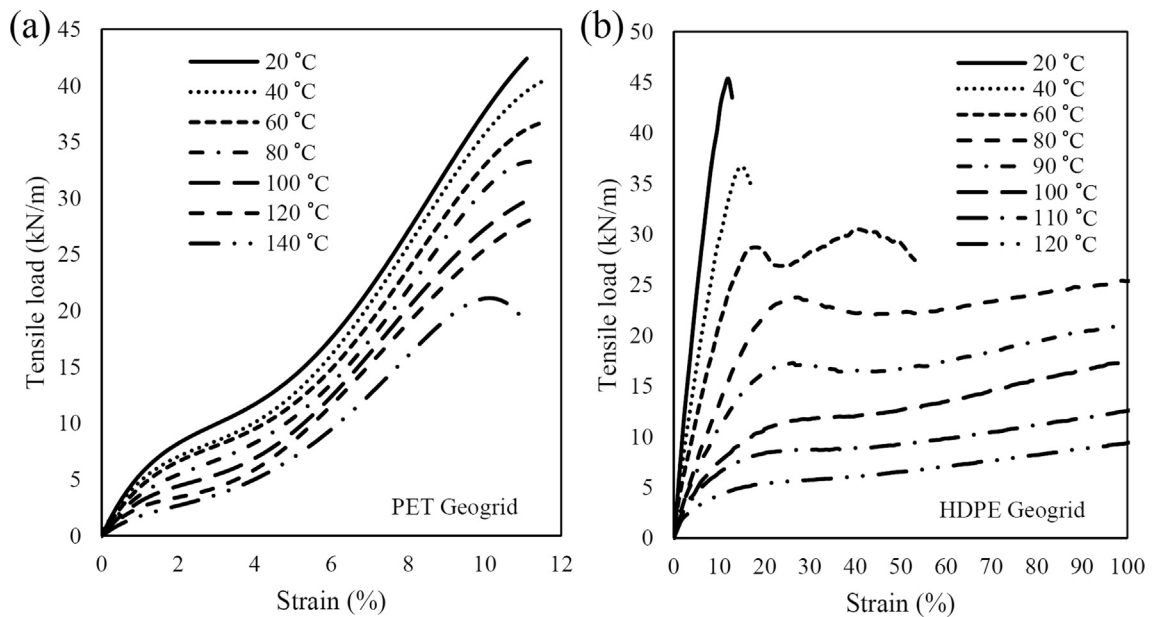

Fig. 4. Typical tensile load versus strain curves at different temperature (a: PET geogrid, b: HDPE geogrid).

2.3.2. Fire resistance tests

The results of the fire tests are summarized in Table 2. The temperature gradient in the soil backfill was regular for all tests. From Table 2 it can be seen that the measured temperatures were higher for the top-row thermocouples, which were placed adjacent to the geogrid layer in the same direction as the horizontal joint of facing.

The bottom row thermocouples were placed behind a concrete block. The existence of joints in the facing can accelerate thermal flow into the backfill. The highest temperature recorded behind the facing was 177 °C on the first test, T1 and was recorded 184 min after the torches were turned off. This indicates that concrete and sand can absorb energy during a fire incident and release

Table 2
Summary of fire resistance tests results.

Test	Time of testing (min)	Type of geogrid	Max. temperature recorded (°C) (behind the facing)		Max. temperature time (min)
			Top row	Bottom row	
T1	357	PET	177	155	305
T2	329	HDPE	166	134	274
T3	332	PET	171	149	278
T4	349	HDPE	162	137	289

the absorbed energy over time. The authors believe that this effect was not considered in Austin [13], who recorded temperatures just after the furnace was turned off (at 30 min).

3. Finite element analysis

Finite element (FE) analysis was conducted to simulate the behavior of a GRS bridge abutment under fire loading. To perform the analysis a plane strain coupled temperature-displacement transient thermal model was created. Some laboratory test results were used as model inputs for FE analysis.

3.1. Initial and boundary conditions

Eq. (1) shows the governing equation (partial differential (heat conduction)) for nonlinear heat conduction in solids. When temperature-dependent materials are used, the aforementioned equation is nonlinear and a more complex model is needed. In this study, ABAQUS software [25] was used for coupled temperature-displacement transient thermal analysis.

$$\rho \cdot C_P(T)\frac{dT(x,t)}{dt} = \frac{d}{dx_i}\left(k(T) \cdot \frac{dT(x,t)}{dx_i}\right) \qquad (1)$$

where $T(x, t)$ is the current spatial temperature field and x is the spatial location vector, $k(T)$ is temperature-dependent thermal conductivity, $C_p(T)$ is temperature- dependent mass heat capacity, and ρ is solid density.

In transient thermal analysis, an initial temperature ($T_{initial}$), a far boundary where temperature remains constant, a thermal boundary to apply thermal load, and an adiabatic boundary must be defined. In this study, the thermal boundary was the external surface of the facing. The fire load (thermal load) was applied to the facing. The fire curve was determined according to the equation recommended in Eurocode 1 for a hydrocarbon fire curve [24] (see Eq. (2)).

$$T = 1080(1 - .0325e^{-.0167t} - 0.675e^{-2.5t}) + 20 \qquad (2)$$

where T is the temperature in the heating phase of a fire in degrees Celsius and, t is the time in minutes. The cooling phase of the fire curve was chosen as a linear function adopted from a RABT-ZTV standard fire curve [26], which shows fire temperature decrease linearly from 1100 °C to 20 °C in 90 min after the heating phase.

3.2. Material modeling

The soil was modeled as an elastic plastic material using the Mohr-Coulomb plasticity model with a non-associated flow rule. The elastic model was used to simulate the modular blocks and bridge seat (sill). For reinforcement, a 3-node 2-D thermally coupled truss element (T2D3T) was used. For the modular blocks, bridge seat (sill) and backfill soil, an 8-node Quadratic Plane Strain Coupled Temperature-Displacement element (CPE8T) were used. Table 3 shows the mechanical parameters of soil, modular blocks and bridge seat (sill) used in the numerical model.

An elastic-plastic temperature-dependent model, which includes material hardening and failure, was used to simulate the behavior of the geogrids. This temperature-dependent model was comprised of nonlinear stress-strain behavior, referred to in ABAQUS as isotropic elasto-plasticity constitutive model. In this model, the mechanical strain rate decomposed into an elastic part and a plastic (inelastic) part [25]. Therefore, small portion of geogrid stress-strain curve was considered to behave elastically (i.e. at strains less than 1%). Table 4 shows the mechanical properties of geogrids which are used in the numerical modeling. The stiffness and yield strength of geogrid are thermal dependent.

To evaluate the efficiency of this model, the response of the geogrids under tensile loading (in air) at different elevated temperatures was determined and compared to the experimental results. Figs. 5 and 6 show the calculated and measured response of the PET and HDPE geogrids under tensile loading at 20 °C, 60 °C, and 100 °C. As shown in Figs. 5 and 6, the FE-based model and the experimental results are in agreement. The FE-based model showed a higher strain at temperatures beyond 80 °C for the PET geogrid. The responses of the model at elevated temperatures (up to 80 °C under almost 10% strain) are in agreement with the tests results. For the HDPE geogrid, the model and the test results for different temperatures were in agreement. Due to the inability of the model to simulate post peak-point behavior, the simulation was continued up to the peak point of the curves.

Table 3
Mechanical properties of soil, modular blocks, and sill used in the finite element analysis.

Material	γ (KN/m^3)	E (MN/m^3)	υ	$\phi°$	$\psi°$	C (KN/m^2)
Backfill (sand)	17.23	20	0.3	34	6	3
Bridge seat (sill)	23.5	20,000	0.21	–	–	–
Facing blocks	23.5	13,800	0.21	–	–	–

Table 4
Mechanical properties of geogrids used in the finite element analysis.

Geogrid type					
PET			HDPE		
Temperature (°C)	Tensile stiffness[a] (KN/m)	Yield strength (KN/m)	Temperature (°C)	Tensile stiffness[a] (KN/m)	Yield strength (KN/m)
20	542.25	42.40	20	553.06	43.86
40	482.74	40.38	40	427.48	36.61
60	432.94	36.88	60	326.55	27.75
80	361.90	33.25	80	191.54	23.62
100	303.99	29.61	90	153.23	13.06
120	251.72	28.09	100	139.07	11.22
140	174.50	21.07	110	122.76	8.27
–	–	–	120	108.39	5.11
γ (KN/m^3)	υ (Poisson's ratio)		γ (KN/m^3)		υ (Poisson's ratio)
5	0.3		3		0.3

[a] Tensile stiffness (E.t) at ε = 1% (E = secant modulus of reinforcement, t=thickness of reinforcement).
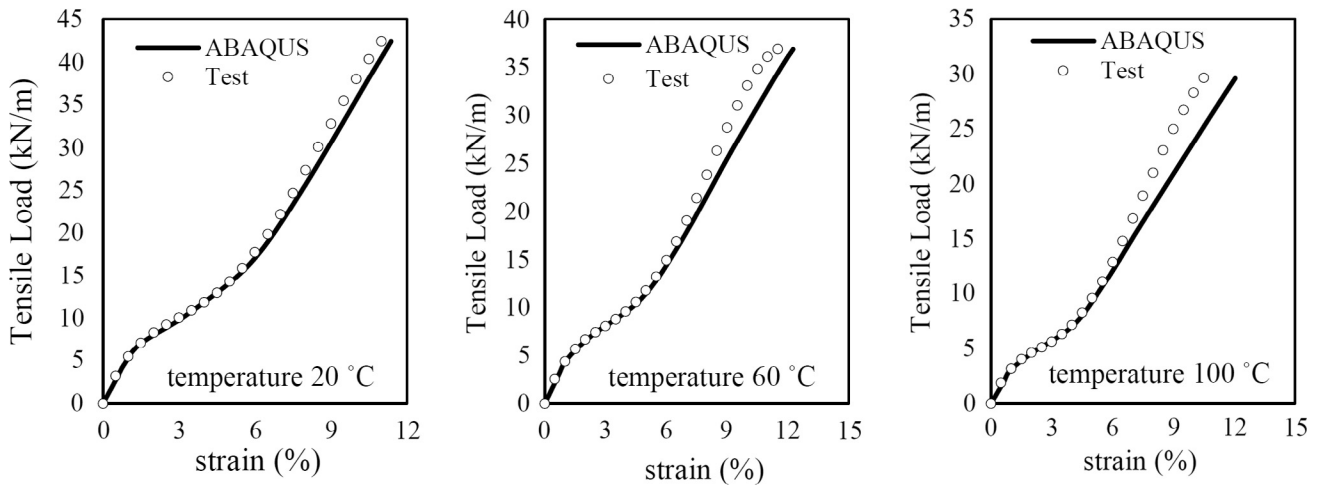
Fig. 5. Measured and calculated tensile test results on PET geogrid at elevated temperature.
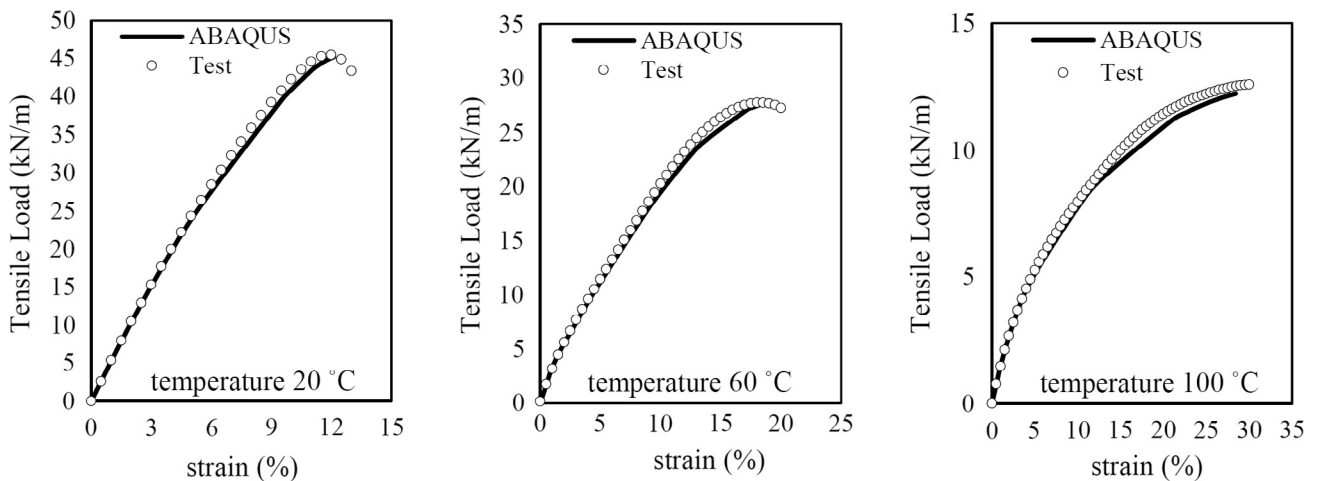

Fig. 6. Measured and calculated tensile test results on HDPE geogrid at elevated temperature.

The soil-block, block-block, and soil-bridge seat interfaces were modeled using interface elements with no cohesion and frictional coefficients equal to 0.4, 0.7, and 0.4, respectively. The geogrid reinforcements (truss elements) extended all the way to the facing and were tied to the facing blocks (to represent the mechanical connection at the modular block facing) and also tied to the soil elements, thus sliding between soil and reinforcement was neglected for these simulations. This assumption is reasonable because under working load conditions for the combination of reinforcement products and compacted sand, soil-reinforcement sliding is small and can be ignored [27–29]. On the other hand, study by Frost and Karademir [30] shows that increasing the temperature within the soil can reduce the likelihood of soil-reinforcement sliding. They investigated the effect of temperature on soil-geosynthetic interface strength. According to their findings, increasing the temperature results in decreasing the surface hardness of geosynthetics and consequently leads to an increase in the friction angle at the interface.

Given that geogrids are buried in the soil, the thermal properties of geogrids (thermal conductivity, k, mass heat capacity, C_p) were assumed to be equal to the backfill (sand), making heat transfer within the backfill and geogrid the same. This is an acceptable assumption as the thermal conductivities of high-density polyethylene and polyester are close to thermal conductivity of sand

[31]. Additionally, Murray and Farrar [10] stated that geosynthetics does not have a remarkable role in heat transfer within the backfill. It is because the cross-sectional area of geosynthetic is very small compared to that of the entire zone of soil backfill.

In this study, a back analysis was conducted to calibrate the thermal properties of sand and concrete (modular block). The fire resistance test, T1, was simulated using finite element method. Prior to the back analysis, the thermal properties of sand and concrete were compiled from literature. The adapted parameters were used as initial estimates for the numerical models. In the first attempt to determine model sensitivity, all of the thermal properties were assumed to be constant, except for one parameter, which was varied to investigate its effect on the response of the model. According to the results, the model was more sensitive to the thermal properties of concrete (modular blocks). It was found that changing the thermal conductivity and the mass heat capacity of concrete affects the temperature-time curve as well as the maximum temperature calculated at different distances within the soil. The numerical results were not in agreement with experimental findings (more specifically for the time-temperature curve) when the constant values were used. In this study thermal conductivity and the specific heat of the sand were estimated from temperature-dependent Equations (see Eqs. (3) and (4)) proposed by Enninful [32] and Pourhashemi et al. [33].

$$k(T) = 0.0006T + 0.0661 \qquad (3)$$

$$c(T) = 40.612T^{0.52} \qquad (4)$$

where $k(T)$ is the temperature-dependent thermal conductivity in W/m·K, ($k_{initial}$ = 0.24 W/m·K), $c(T)$ is the temperature-dependent specific heat in J/kg·K, ($c_{initial}$ = 778 J/kg·K), T is the temperature in Kelvin.

The thermal and mechanical properties of concrete (normal strength) such as specific heat, conductivity, elastic modulus, and stress-strain relationship are temperature-dependent and change significantly at high temperatures. However, in this study, apart from thermal conductivity and mass heat capacity, other

concrete and sand properties were not considered temperature-dependents.

For FE analysis, these properties were estimated according to suggestions made by Harmathy et al. [34,35], ASCE [36], and Eurocode 2 [37]. Figs. 7 and 8 show the temperature-dependent thermal conductivity (λ_C) and specific heat (C_C) of concrete adopted from the aforementioned resources. In these figures, thermal properties, which lead to the best agreement between the numerical and measured results, also have been shown. Fig. 9 displays the results of the test-calibrated FEM thermal model and the fire test, T1. It should be mentioned that d in Fig. 9 is the distance from the facing. However, in order to ensure that the results of plane strain model are numerically reliable, a three dimensional finite element
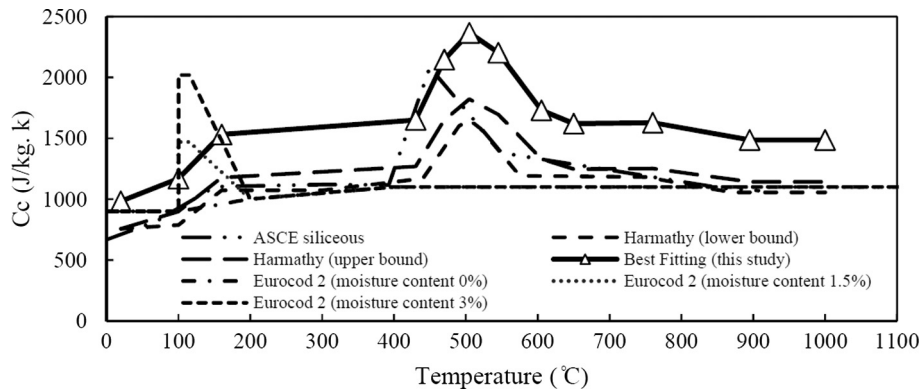

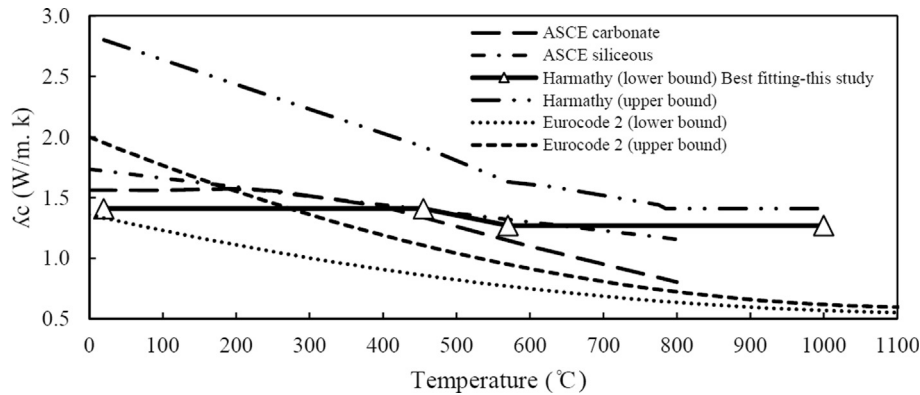Fig. 7. The temperature-dependent specific heat (C_C) of normal-strength concrete.

Fig. 8. The temperature-dependent thermal conductivity (λ_C) of normal-strength concrete.
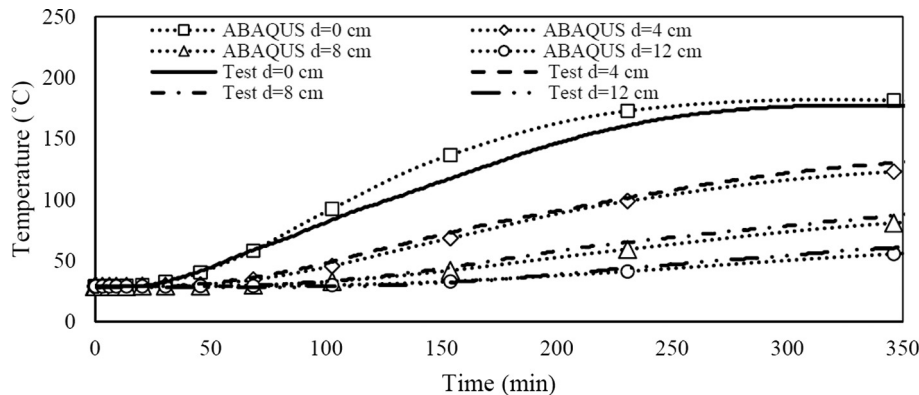

Fig. 9. Temperature change within the soil backfill, the test-calibrated FEM thermal model vs. test results.

analysis was also conducted. The three dimensional analysis showed that the temperature changes within the soil backfill were close to those obtained using the plane strain analysis (less than 8% difference). Additionally, the facing lateral displacements obtained using 2D analysis was checked against 3D analysis and less than 12% difference was observed which is in good agreement with the findings of Helwany et al. [19]. The plane strain analysis involves much less degree of freedoms making it more desirable for the analysis.

4. Parametric analysis

Forty analyses were carried out to study the performance of modular block facing GRS bridge abutments subjected to hydrocarbon fire scenario. Variables include (a) Sill pressure: 50, 100, 150, and 200 kPa, (b) fire duration time (the heating phase): 60, 120, 180, 240, and 300 min, (c) type of geogrid and (d) block width, 20, and 28 cm (default case). The allowable bearing pressure of a bridge sill over reinforced soil retaining walls was limited to 200 kPa in accordance with FHWA [23].

4.1. Model geometry, mesh, and boundary conditions

The GRS bridge abutment geometry used in the parametric analysis is shown in Fig. 10. This geometry is similar to the GRS bridge abutment with an isolated sill that Wu et al. [38] used in their study, except that only the load of upper wall (the wall

behind the bridge seat with a height of 2.44 m) was applied in the model. The dimensions and parameters of the geometry are as follows:

Wall height = 4.80 m.
Sill height = 0.75 m.
Sill clear distance (between front edge of sill to back face of facing blocks) = 0.15 m.
Reinforcement length = 5.00 m.
Reinforcement spacing = 0.30 m.
Modular block dimensions = 0.15 m × 0.28 m × 0.20 m (height × width × length).

The mechanical and thermal boundary conditions were applied to the model as shown in Fig. 10. A fixed horizontal displacement boundary condition at the right edge of the model and a fixed vertical displacement boundary condition at the bottom of the model were used as mechanical boundaries. As can be seen from Fig. 10, the toe of the facing column is restrained horizontally by a spring element. The stiffness of this spring was 7 MN/m/m. Previous research showed that the existence of a stiff horizontal toe at the bottom of the facing column plays an important role in the numerical equilibrium of GRS walls [39]. In this study, an initial temperature of 20 °C was applied to all parts of the model. The vertical far boundary was selected 5 m behind the facing at the end of the reinforced zone. The fire curves used in the analysis can be seen in Fig. 11.
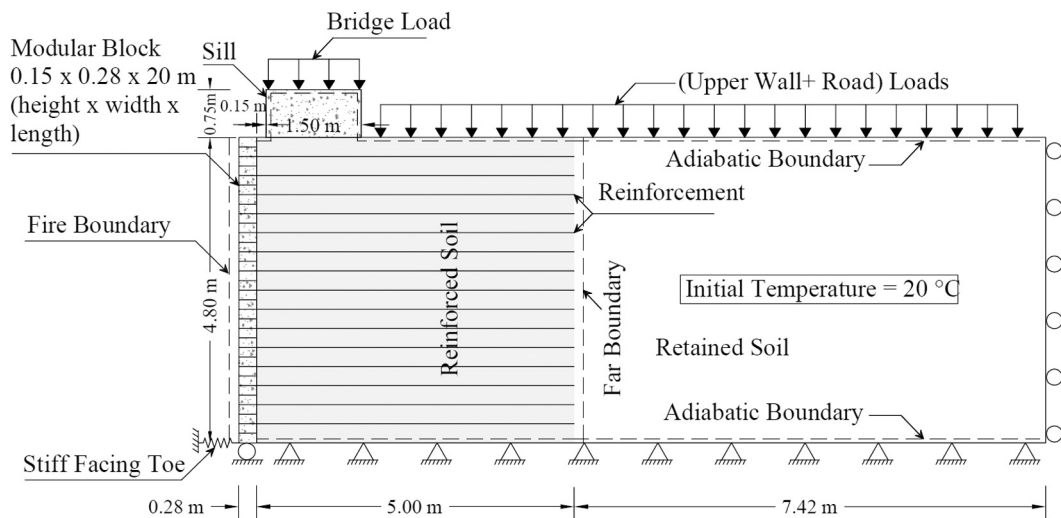

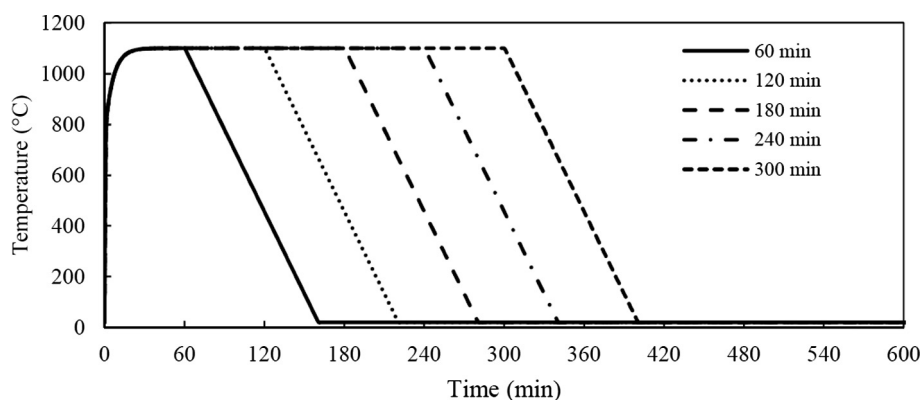**Fig. 10.** GRS bridge abutment geometry used in the parametric analysis.

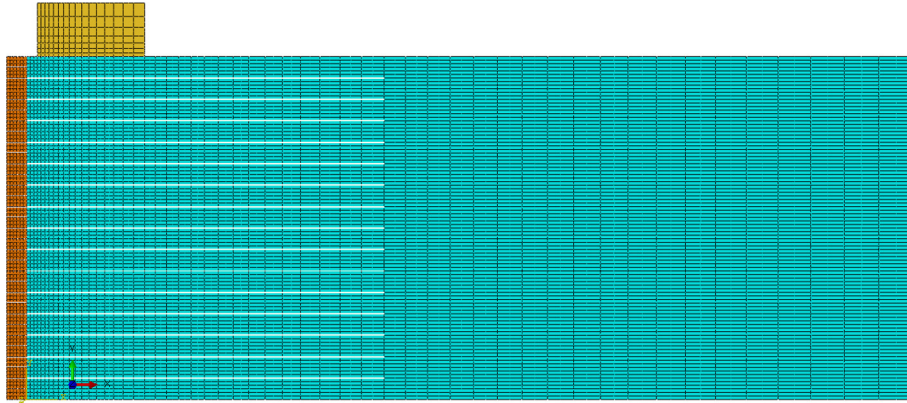**Fig. 11.** Fire curves with different time duration used in parametric analysis.

Fig. 12. Model-generated mesh before analysis.

A parametric analysis was conducted on the mesh sizing to determine the optimal mesh density, which for the purpose of brevity is not mentioned here. The generated mesh, after sensitivity analysis, can be seen in Fig. 12. The final FE mesh used in this study consisted of 19,497 nodes and 6376 elements (5776 CPE8T, and 600 T2D3T). As shown in this figure, in the vicinity of the facing, the mesh is refined mainly because it is the most important heat-induced influenced zone in the model.

5. Main results and discussion

5.1. Temperature distribution within the soil backfill

Maximum temperatures occurred at various distances within the soil backfill behind the facing as shown in Fig. 13. This Figure suggests that the maximum temperature at different distances within the soil backfill increases with increased fire duration. The maximum temperature determined in the soil backfill, just behind the facing, was 58 °C with a fire duration of 60 min, and 123 °C with a fire of 300 min. Results show that the depth of the soil backfill affected by a fire is almost 50 cm. Overall, according to the experimental and numerical findings of this study for fire duration up to 300 min and block thicknesses of 15 cm, 20 cm (to be discussed later) and 28 cm, the fire-induced influenced zone of the soil is considerable up to 50 cm behind the concrete blocks. It should be mentioned that the thickness of concrete blocks affects the backfill soil influenced by the fire; however, for the aforementioned thicknesses used in this study, the change in temperature within the soil backfill beyond 50 cm was not significant.
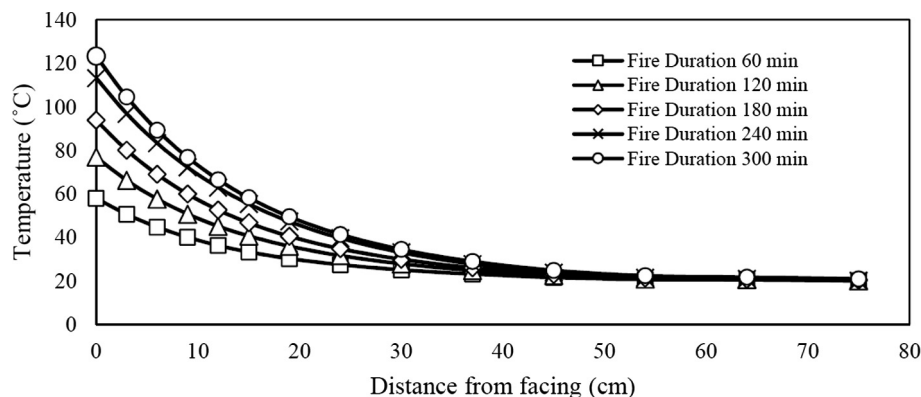
Fig. 14 displays examples of temperature contours within the model under two aforementioned fire scenarios. It should be mentioned that the contours were obtained when the maximum temperature occurred (58 °C and 123 °C).

5.2. Facing lateral displacement

Figs. 15 and 16 display the facing lateral displacement (in the levels of geogrid layers) for different fire durations and different sill pressures. These figures suggest that, under all loading conditions, increased fire duration causes greater facing lateral displacement. This is expected because the tensile strength and elastic modulus of the geogrids decreases as temperature increases (Section 2.3.1). The facing deformation curves were different for each type of geogrid. The tensile strength tests for geogrids showed that HDPE geogrids are more sensitive to elevated temperatures. Under a 100 kPa applied pressure for abutment reinforced with HDPE geogrids, maximum lateral displacements are 29.39 mm for non-fire conditions and 41.93 mm for 300 min fire (an increase of 43%). These values were 31.8 mm and 37.33 mm, respectively, for abutment reinforced with a PET geogrid (an increase of 17%).

The increase in displacement from the fire became more pronounced as the applied pressure increased. Under 50 kPa sill pressure, the lateral displacements of the abutment reinforced with HDPE geogrids were18.68 mm for the non-fire condition and 23.73 mm for 300 min fire. This indicates a 27% increase in facing lateral displacement. Under 200 kPa sill pressure, these values were 52.92 mm for the non-fire condition, and 72.09 mm for 300 min fire, an increase rate of 36%. Under the same conditions,
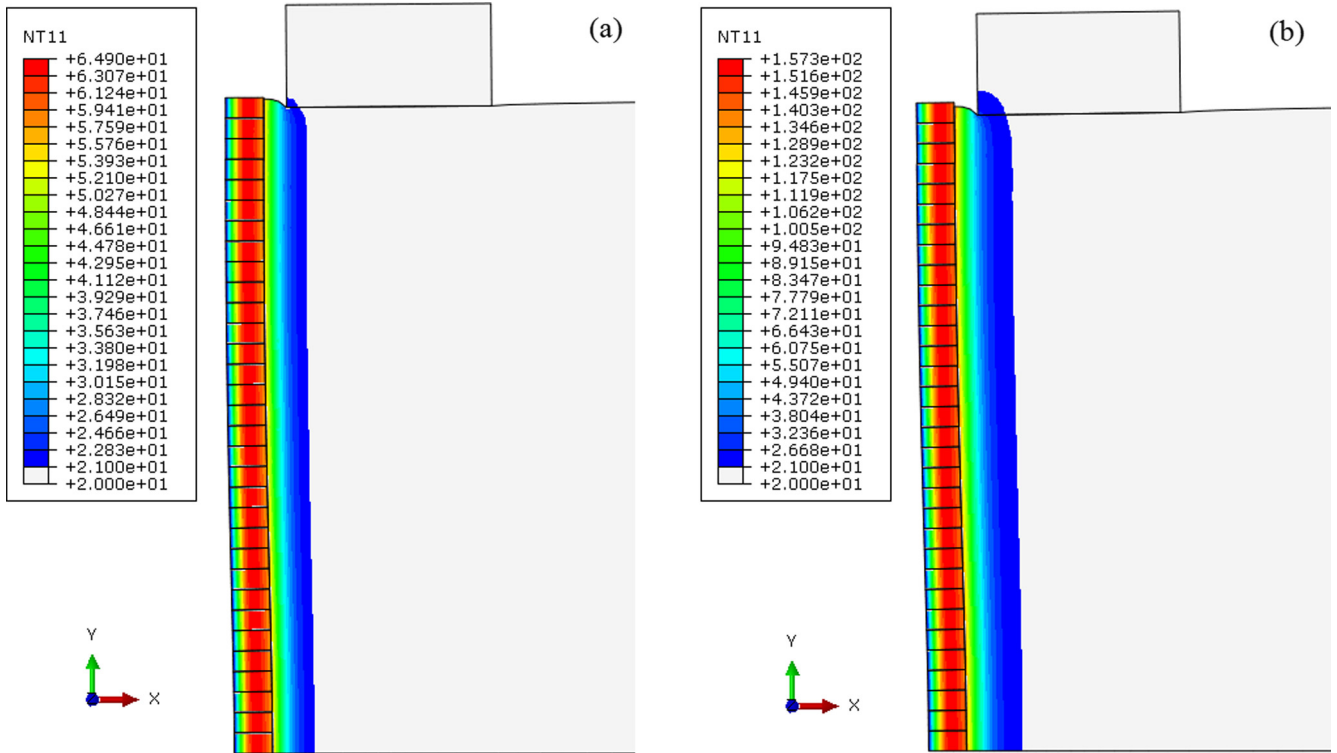

Fig. 13. Maximum temperatures occurred at different distances behind the facing.

Fig. 14. Temperature contours within the model, (a) fire duration of 60 min, (b) fire duration of 300 min.
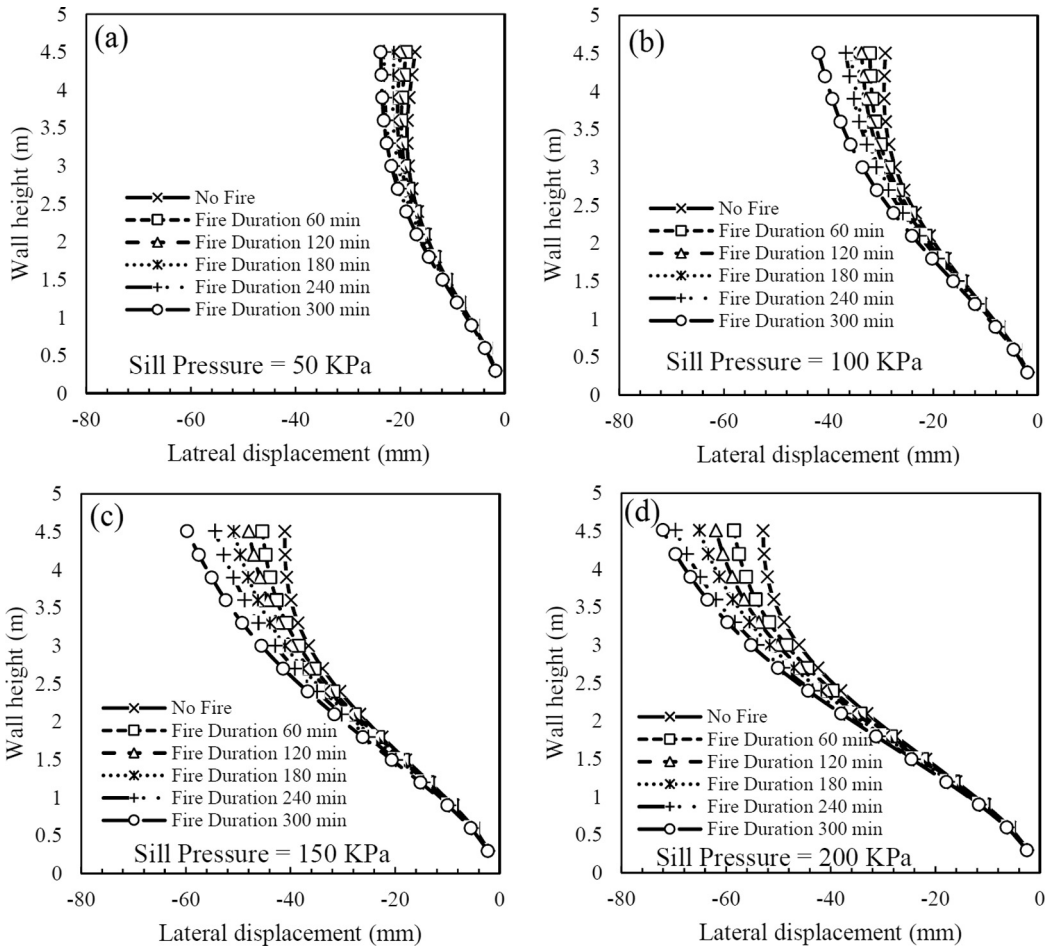

Fig. 15. Post fire lateral displacement of the facing for bridge abutment reinforced with HDPE, (a) sill pressure = 50 kPa; (b) sill pressure = 100 kPa; (c) sill pressure = 150 kPa; (d) sill pressure = 200 kPa.

Fig. 16. Post fire lateral displacement of the facing for bridge abutment reinforced with PTE, (a) sill pressure = 50 kPa; (b) sill pressure = 100 kPa; (c) sill pressure = 150 kPa; (d) sill pressure = 200 kPa.
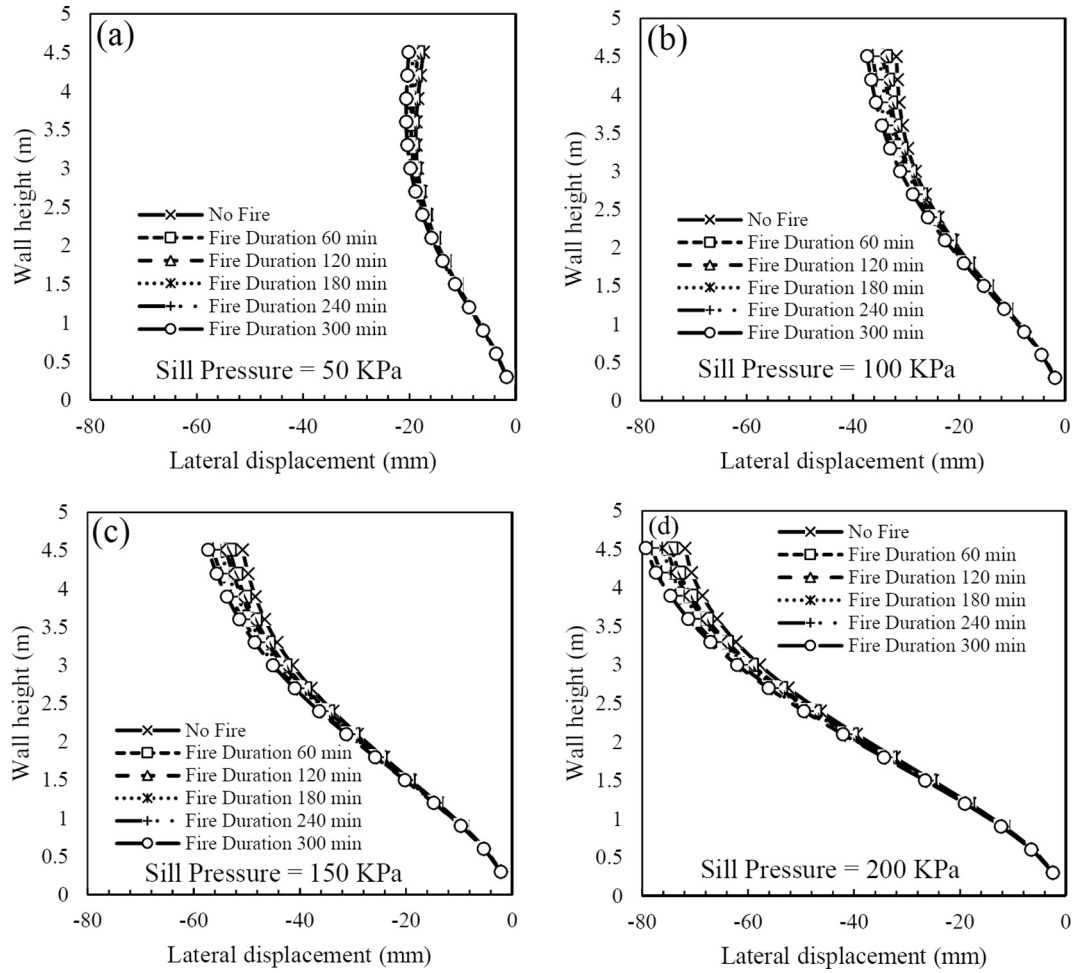
the increases in facing lateral displacement for abutment reinforced with PET geogrid were 9.8% and 10%, respectively.

As shown in these figures, at the same pressures and under non-fire conditions, the facing lateral displacement of the GRS bridge abutment reinforced with PET geogrids was higher. A possible reason for this is that at a strain range of 1.5–5%, the secant modulus

of the PET geogrid is immediately reduced before rising again. The secant modulus of the HDPE geogrid shows no significant reduction until failure (see Fig. 4). Under 50 kPa sill pressure (low pressure), the calculated facing displacement curves were approximately equal. Overall, Figs. 15 and 16 suggest that when the fire exceeded 60 min, facing lateral displacements become
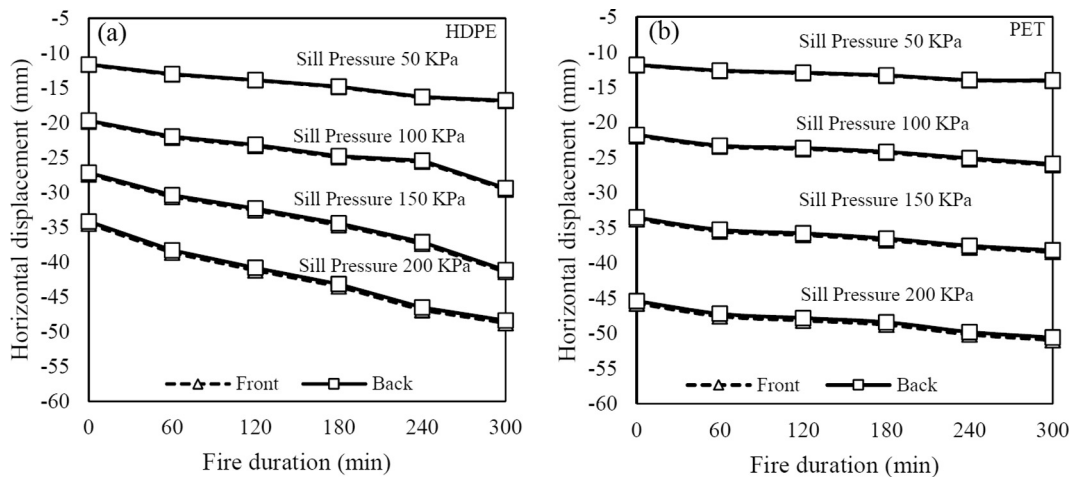

Fig. 17. Relationship between applied pressure, fire duration, and sill horizontal displacement, (a: bridge abutment reinforced with HDPE, b: bridge abutment reinforced with PTE).

more pronounced. The presented deformations in Figs. 15 and 16 are due to soil, geogrid and facing block interactions.

5.3. Bridge seat (sill) displacements

Figs. 17 and 18 show the effects of sill pressure and fire duration on the horizontal and vertical displacements of the bridge seat (sill). These figures suggest that under non-fire conditions the vertical and horizontal displacement of the bridge seat (sill) increase as sill pressure increases. It was also observed that an increase in fire duration caused more bridge seat deformation.

Comparing the vertical and horizontal displacement curves for the two types of abutments shows that the slope of the displacement curves is higher for abutments reinforced with a HDPE geogrid. This is not surprising as the performance of the HDPE geogrid at elevated temperatures is weaker than the PET geogrid. A simple comparison between the graphs of Fig. 18 indicates that as the fire duration increases, the bridge sill starts to settle non-uniformly (the front part of the sill settles more). This leads to bridge sill rotation. The abutment reinforced with a HDPE geogrid showed greater sill rotation (see Fig. 18) than abutment reinforced with a PET geogrid.

5.4. Effects of block width

The effect of the block width on GRS bridge abutments subjected to fire loading was investigated using blocks with a width of 28 cm (default case) and 20 cm. The width of 20 cm block was the minimum width of a modular block facing recommended by FHWA [23]. Fig. 19 displays the additional facing lateral displacement from the fire loading of bridge abutments reinforced with (a) HDPE and (b) PET geogrids, with a fire duration of 120 min and sill pressure of 100 kPa. The maximum additional facing lateral displacement of the abutment with block width of 20 cm is much higher than the abutment with block width of 28 cm (almost twice as great). This is because decreasing the width of the block leads to an increase in the temperature behind the facing and a reduction in tensile strength as well as elastic modulus of geogrids. Based on the numerical results, the maximum temperature that occurred just behind the facing (28-cm width) was 77 °C for the 120 min fire (see Section 5.1). For the facing with a width of 20 cm, this value was 117 °C, an increase of 52%. Fig. 19 shows that the additional facing lateral displacement of the GRS bridge abutments are greater when the HDPE geogrid was used instead of the PET geogrid.
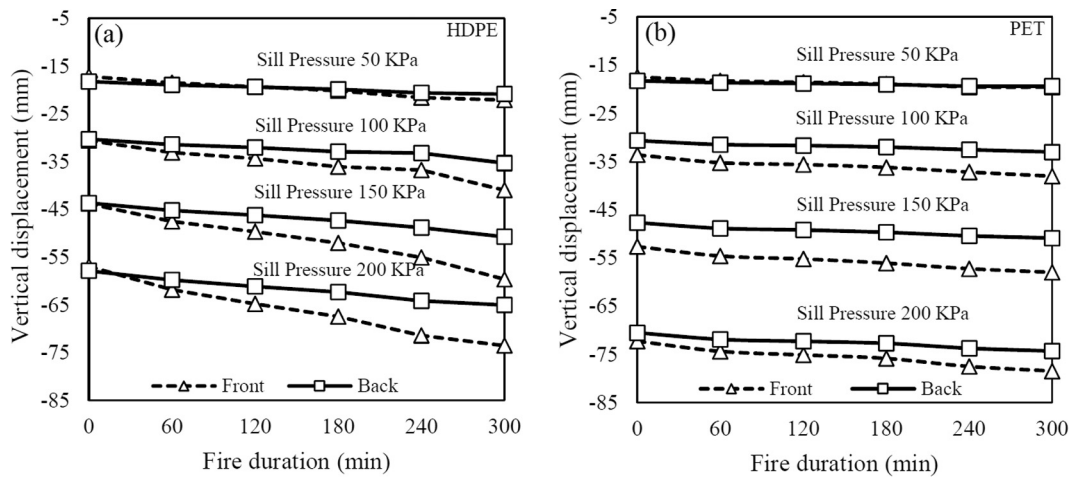

Fig. 18. Relationship between applied pressure, fire duration, and sill vertical displacement, (a: bridge abutment reinforced with HDPE, b: bridge abutment reinforced with PTE).
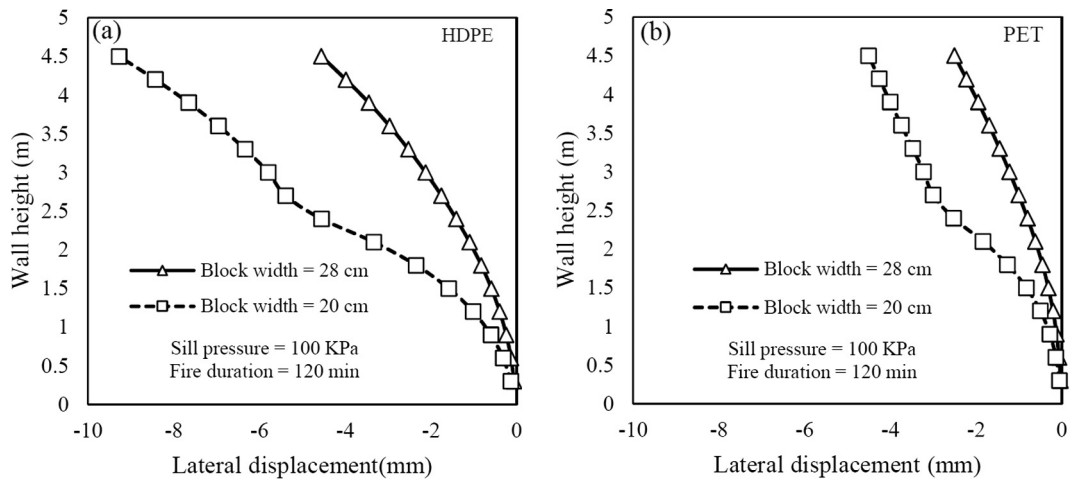

Fig. 19. Additional facing lateral displacement due to fire loading, (a) HDPE geogrid; (b) PET geogrid.

6. Conclusions

In this study, some experimental and numerical tests were performed to investigate the effects of fire on the behavior of GRS bridge abutments. Laboratory tests were: (a): tensile test under elevated temperatures for two types of geogrids and, (b): fire resistance tests on a physical model of reinforced soil structures with modular block facing exposed to a hydrocarbon fire curve. Using experimental results, a numerical FE-based model was calibrated and a parametric study was carried out to investigate the performance of GRS bridge abutments. Based on this study, the following conclusions are made:

(1) Based on this study, it was found that fire could lead to elevated temperatures within the soil backfill (as expected), reducing the tensile strength and elasticity modulus of the geosynthetic and causing higher deformation in the facing and bridge seat. Deformations were not remarkable for fire durations under 60 min.

(2) The results showed that the depth within the soil backfill affected by a fire is about 50 cm behind the modular block facing. In this area, the temperature within the soil backfill decreases in a nonlinear manner as the facing becomes more distant.

(3) Facing lateral displacements were different for each type of geogrid. It was found that the HDPE geogrid are more sensitive to elevated temperatures in comparison with the PET geogrid and the facing lateral displacement of bridge abutments reinforced with the HDPE geogrid was higher for the same fire conditions.

(4) This study showed that sill pressure and fire duration affect the performance of GRS bridge abutments. The facing deformation, vertical and lateral displacement of the bridge seat increase with increases in sill pressure and fire duration.

(5) Based on the findings, the width of blocks is an important factor, which can affect the performance of GRS bridge abutments. As the width of blocks increases, the maximum temperature behind the facing reduces and consequently the facing lateral displacement decreases.

Acknowledgment

References

[1] Budiman J. Effects of temperature on physical behavior of geomembrane. In: Proc of the 5th int conf geotextiles, geomembranes, and related products. IGS, USA. p. 1093–6.

[2] Hsuan YG, Koerner GR, Koerner RM. Field measurements of oxygen, temperature and moisture behind segmental retaining walls. In: Int geosynth conf. p. 1431–4.

[3] Li M, Hsuan YG. Temperature and pressure effects on the degradation of polypropylene tape yarns—depletion of antioxidants. J Geotext Geomembr 2004;22(6):511–30.

[4] Zornberg JG, Byler BR, Knudsen JW. Creep of geotextiles using time–temperature superposition methods. J Geotech Geoenviron Eng 2004;1:1158–68.

[5] Hsieh C, Tseng Y. Tensile creep behavior of a PVC coated polyester geogrid at different temperatures. J GeoEng 2008;3(3):113–9.

[6] Rowe RK, Rimal S, Sangam H. Ageing of HDPE geomembrane exposed to air, water and leachate at different temperatures. J Geotext Geomembr 2009;27:137–51.

[7] Kongkitkul W, Tabsombut W, Jaturapitakkul C, Tatsuoka F. Effects of temperature on the rupture strength and elastic stiffness of geogrids. J Geosynth Int 2012;19(2):106–23.

[8] Kasozi AM, Siddharthan RV, Mahamud R. Temperature distribution in mechanically stabilized earth wall soil backfills for design under elevated temperature conditions. J Therm Sci Eng Appl 2015:021004.

[9] Segrestin P, Jailloux JM. Temperature in soils and its effect on the ageing of synthetic materials. J Geotext Geomembr 1988;7:51–69.

[10] Murray RT, Farrar DM. Temperature distributions in reinforced soil retaining wall. J Geotext Geomembr 1988;7:33–50.

[11] ASTM D6637. Standard test method for determining tensile properties of geogrids by the single or multi-rib tensile method. ASTM International, West Conshohoken, PA, USA; 2015.

[12] Wright W, Lattimer B, Woodworth M, Nahid M, Sotelino E. Guide specification for fire damage evaluation in steel bridges. NCHRP, PN. 12–85, TRB; 2013.

[13] Austin RA. The effect of installation activities and fire exposure on geogrid performance. J Geotext Geomembr 1997;15:367–76.

[14] Bathurst RJ, Karpurapu RG, Jarrett PM. Finite element analysis of a geogrid reinforced soil wall. ASCE GSP 30: grouting, soil improvement and geosynthetics, vol. 2. p. 1213–24.

[15] Karpurapu RG, Bathurst RJ. Behaviour of geosynthetic reinforced soil retaining walls using the finite element method. J Comput. Geotech 1995;17(3):279–99.

[16] Rowe RK, Ho SK. Continuous panel reinforced soil walls on rigid foundations. J Geotech Geoenviron Eng 1997;123(10):912–20.

[17] Rowe RK, Ho SK. Horizontal deformation in reinforced soil walls. Can Geotech J 1998;35(2):312–27.

[18] Helwany SMB, Reardon G, Wu JTH. Effects of backfill on the performance of GRS retaining walls. J Geotext Geomembr 1999;17:1–16.

[19] Helwany SMB, Wu JTH, Kitsabunnarat A. Simulating the behavior of GRS bridge abutments. J Geotech Geoenviron Eng 2007;133(10):1129–240.

[20] ASTM D4254: standard test methods for minimum index density and unit weight of soils and calculation of relative density. ASTM International, West Conshohoken, PA, USA; 2014.

[21] ASTM D4253. Standard test methods for maximum index density and unit weight of soils using a vibratory table. ASTM International, West Conshohoken, PA, USA; 2010.

[22] ASTM D3080. Standard test method for direct shear test of soils under consolidated drained conditions. ASTM International, West Conshohocken, PA, USA; 2011.

[23] Elias V, Christopher BR, Berg RR. Mechanically stabilized earth walls and reinforced soil slopes design and construction guidelines. Report no FHWA-NHI-00-043, Federal Highway Administration; 2001.

[24] ENV. Eurocode 1. Actions on structures - Part 1–2: General actions - actions on structures exposed to fire, 1991-2-2, The European Union per Regulation; 2002.

[25] ABAQUS 6.11. Providence (RI, USA): Dassault Systèmes Simulia Corp.

[26] www.promat-tunnel.com/ Tunnel Fire Protection/ fire curves.

[27] Ambauen SJ. Numerical simulation of mechanically stabilized earth walls for parametric evaluation of behavior under surcharge loading. MSc thesis, Oregon State Univ, USA; 2014.

[28] Fox PJ, Shing PB, Zheng Y. Interaction of GRS abutments with bridge superstructures under seismic loading (Phase I). Report no SSRP 15-01, Dept Struct Eng Univ of California, San Diego La Jolla, California; 2015.

[29] Bathurst RJ, Hatami K. Seismic response analysis of a geosynthetic reinforced soil retaining wall. J Geosynth Int 1998;5(1–2):127–66.

[30] Frost JD, Karademir T. Apparatus for geosynthetic interface testing and evaluation under elevated temperature conditions. J Test Eval 2013;41(2):1–11.

[31] Mark JE, editor. Physical properties of polymers handbook. New York: Springer; 2007.

[32] Enninful EK. Predicting temperatures profiles during simulated forest fires. MSc thesis. University of Saskatchewan, Saskatoon, SK; 2006.

[33] Pourhashemi SA, Hao OJ, Chawla CR. An experimental and theoretical study of the non-linear heat conduction in dry porous media. Int J Energy Res 1999;389–401.

[34] Harmathy TZ. Properties of building materials at elevated temperatures. Division of Building Research. DRP paper no 1080; 1983.

[35] Harmathy TZ. Properties of building materials. In: SFPE handbook of fire protection engineering. p. 378–91.

[36] Lie TT. Structural fire protection. Reston (VA): American Society of Civil Engineers; 1992.

[37] ENV. Eurocode 2. Design of concrete structures - Part 1–2: General rules - structural fire design, 1992-1-2, The European Union per Regulation; 2004.

[38] Wu JTH, Lee KZZ, Pham T. Allowable bearing pressures of bridge sills on GRS abutments with flexible facing. J Geotech Geoenviron Eng 2006;132(7):830–41.

[39] Huang B, Bathurst RJ, Hatami K. Numerical study of reinforced soil segmental walls using three different constitutive soil models. J Geotech Geoenviron Eng 2009;135(10):1486–98.